Broadband impedance calculations and single bunch instabilities estimations of of the HLS-II storage ring *

ZHANG Qing-Kun(张青鹍)[1)] WANG Lin(王琳)[2)] LI Wei-Min(李为民)[3)] GAO Wei-Wei(高巍巍)[4)]
NSRL, School of Nuclear Science and Technology, University of Science and Technology of China, Hefei 230029, China

Abstract: The upgrade project of the Hefei Light Source storage ring is under way. In this paper, the broadband impedances of resistive wall and coated ceramic vacuum chamber are calculated using the analytic formula, and the wake fields and impedances of other designed vacuum chambers are simulated by CST code, and then a broadband impedance model is obtained. Using the theoretical formula, longitudinal and transverse single bunch instabilities are discussed. With the carefully-designed vacuum chamber, we find that the thresholds of the beam instabilities are higher than the beam current goal.

Key words: wake fields, broadband impedance, CST, single bunch instabilities

PACS: 29.20.D-, 29.27.Bd **DOI:** 10.1088/1674-1137/39/12/127004

1 Introduction

The Hefei Light Source (HLS) is a dedicated VUV and soft X-ray light source, with beam energy of 800 MeV and storage ring circumference of 66.13 m. To improve the quality of synchrotron radiation, an important upgrade project of the HLS is underway, where the storage ring will be reconstructed. The main parameters of the HLS-II storage ring are listed in Table 1. Except for the lower beam emittance, the beam intensity will be higher than before, which is essential for high synchrotron radiation flux and brightness [1].

Because geometric impedance-driven beam collective effects are important considerations for reaching higher beam intensity, it is necessary to calculate the longitudinal impedances of components in the HLS-II storage ring, which may cause longitudinal and transversal bunch instabilities, and to estimate the acceptable beam current.

In this paper, short range wake fields of various vacuum chambers in the HLS-II storage ring are calculated by some analytical method and CST code [2], and then a broadband impedance model is established. Based on the impedance model, single bunch instability thresholds, such as for the microwave instability, and the transverse model coupling instability are estimated using the classical formulas [3, 4].

2 Short review of wake field and impedance

When a charged particle is travelling through a storage ring, if the wall of the beam pipe is not perfectly conducting and has some discontinuities, the movement of the image charges will be slowed down, thus leaving electromagnetic fields behind, which will influence the motion of later particles. We calculate the longitudinal and transverse wake functions by integrating over the EM force normalized by the charge q and a horizontal offset ξ [4, 6]:

$$\begin{cases} W'_{\parallel}=-\dfrac{1}{q}\displaystyle\int_{-\infty}^{\infty}\mathrm{d}zE_z. \\ W_{\perp}=\dfrac{1}{q\xi}\displaystyle\int_{-\infty}^{\infty}\mathrm{d}z(\boldsymbol{E}+\boldsymbol{v}\times\boldsymbol{B})_{\perp}. \end{cases} \tag{1}$$

For a Gaussian bunch, the wake potential can in principle be found from the convolution of the wake function with the normalized line density $\lambda(\tau-t)$.

Actually, we often use the coupling impedance, which is the Fourier transformation of the wake function for analytical study of the beam instabilities. We also use the reduced impedance for the longitudinal beam instabilities, which is a comparable quality for storage rings with different circumferences. The reduced impedance is de-

Received 27 April 2015
* Supported by Natural Science Foundation of China (11175182, 11175180)
1) E-mail: zhangqk@mail.ustc.edu.cn
2) E-mail: wanglin@ustc.edu.cn
3) E-mail: lwm@ustc.edu.cn
4) E-mail: gaoww@ustc.edu.cn

Table 1. Parameters of the HLS-II storage ring.

beam energy/MeV	800
circumference/m	66.13
momentum compaction factor	0.02
transverse beam emittance/nm·rad	37
natural energy spread	0.000472
nominal RMS bunch length/mm	14.8
vacuum chamber height size/m	0.04
synchrotron frequency/kHz	28.0
betatron tunes	(4.4141, 3.2235)
average transverse beta function/m	8.50/5.25
energy loss per turn/keV	16.73
main RF frequency/MHz	204
single beam current $I_{\rm dc}$/mA	300/45
damping time $\tau_x/\tau_y/\tau_z$/ms	23/22/10

fined as the impedance divided by the harmonic number $n=\omega/\omega_0$.

3 Wake fields and impedances for HLS-II storage ring

In the HLS-Ⅱ storage ring, we can ignore the influence of the space charge effect due to the highly relativistic beam [7]. In this section, we consider the resistive wall and the discontinuities of vacuum chambers by analytical formula and by the CST code. The wake potentials were calculated up to s=100 mm, where s is the bunch coordinate. Meanwhile we used a Gaussian bunch with rms bunch length σ_z of 3 mm and charge Q of 0.0000001 C in the CST code. In the wake field solver, all metallic parts were considered to be perfect electric conductors, and open boundary conditions were assigned at the entrance and exit of the structure.

3.1 Resistive wall

The octagonal cross-section of the HLS-Ⅱ storage ring is shown in Fig. 1, including its inner dimensions. Almost all the chambers are made of stainless steel (SS).

The impedance of the resistive wall is calculated analytically. In order to estimate the resistive wall impedance, a simplified model is introduced. Here the whole cross section of the vacuum chamber is considered to be elliptical [8], with a length of major axis $2a$ and minor axis $2b$.

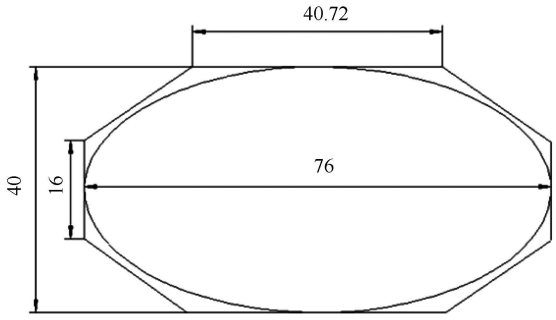

Fig. 1. Cross-section of the SS vacuum chamber. All the dimensions are in units of mm. The pipe shape indicated by the ellipse was used in the impedance estimation.

$$a=d\cosh u_0,\ \ b=d\sinh u_0,\ \ d^2=a^2-b^2, \tag{2}$$

where $2d$ is the distance between the foci, the major and minor semi-axes of the elliptical cross-section are $a=38$ mm and $b=20$ mm, and its eccentricity is given by $\sqrt{1-b^2/a^2}=1/\cosh u_0$.

The longitudinal resistive wall impedance of this elliptic pipe is given by [8, 9]:

$$\frac{Z_{//}}{n}=Z_0\frac{(1+j)}{2}\frac{\delta}{b}\frac{L}{2\pi R}G_0(u_0), \tag{3}$$

where

$$\begin{aligned} G_0(u_0) &= \frac{\sinh u_0}{2\pi}\int_0^{2\pi}\frac{Q_0^2(v){\rm d}v}{[\sinh^2 u_0+\sin^2 v]^{1/2}},\\ Q_0(v) &= 1+2\sum_{m=1}^{\infty}(-1)^m\frac{\cos 2mv}{\cosh 2mu_0},\\ \delta &= \sqrt{\frac{2c}{Z_0\sigma\omega}}=\sqrt{\frac{2\rho_1}{\omega\mu_0}}. \end{aligned}$$

Based on the Panofsky–Wenzel theorem, the transverse resistive wall impedance of an elliptical pipe can be estimated with the effective radius b [10]:

$$Z_\perp=\frac{2R}{b^2}\frac{Z_{//}}{n}. \tag{4}$$

In this case, the conductivity of SS beam pipe is 1.5×10^6 $(\Omega{\rm m})^{-1}$. Then we can obtain the impedances of the resistive wall:

$$\begin{cases} \dfrac{Z_{//}}{n}=4.5212(1+j)/\sqrt{n}\Omega,\\ Z_x=33.865(1+j)/\sqrt{n}\ {\rm k}\Omega,\\ Z_y=36.8767(1+j)/\sqrt{n}\ {\rm k}\Omega. \end{cases} \tag{5}$$

3.2 Coated ceramic vacuum chamber

In the HLS-Ⅱ storage ring, there are four coated ceramic vacuum chambers (Fig. 2) inside the kicker magnets. A metal coasting is required on the inner surface of the ceramic vacuum chamber, the thickness of which will affect the pulsed magnetic field of the kicker magnet and the coupled impedance of the ceramic vacuum chamber. After careful design, the thickness of the metal coasting has been set as 1 μm in the ring. For this kind of structure, it is very difficult to calculate the coupling impedance using CST code, because of the small thickness of the metal coating. Hence a simple model of an infinitely long pipe was used to estimate the coating impedance [9].

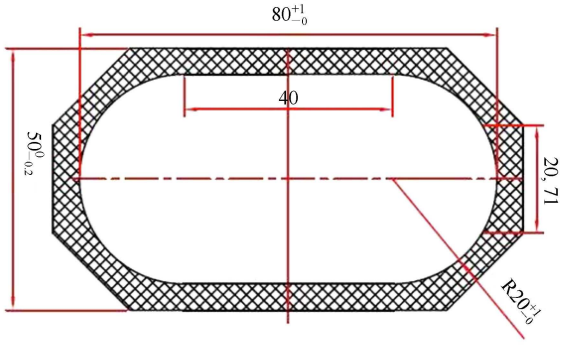

Fig. 2. (color online) Cross section of ceramic vacuum chamber of the injection system at HLS-II.

The longitudinal impedance formula is presented below:

$$\frac{Z_{//}}{L}=Z_{\rm met}\frac{A+\tanh(\kappa d_{\rm m})}{1+\tanh(\kappa d_{\rm m})}, \tag{6}$$

where

$$Z_{\rm met}=\frac{1+i{\rm sgn}(\omega)}{bc}\sqrt{\frac{|\omega|}{2\pi\sigma}}\frac{1}{\sqrt{4\pi\varepsilon_0}},$$

$$A=\frac{(1-i{\rm sgn}(\omega))d_{\rm c}}{d_{\rm s}}\left(1-\frac{1}{\varepsilon}\right),$$

$$\kappa=\frac{1-i{\rm sgn}(\omega)}{\delta},$$

$$d_{\rm s}=\frac{c}{\sqrt{2\pi\sigma|\omega|}}\sqrt{4\pi\varepsilon_0}.$$

In HLS-II, the length of this piece L is 0.28 m, the thickness of the metal layer $d_{\rm m}$ is 10^{-6} m, the thickness of the ceramic chamber $d_{\rm c}$ is 0.005 m, and the equivalent radius of the vacuum chamber is 0.2 m, so we obtain that: $Z_{//}=0.002497n+0.014774j$.

3.3 Beam position monitors

There are 36 Beam Position Monitors (BPMs) in the HLS-II storage ring. Each BPM consists of four button-type electrodes, which are located on the upper and lower planes of the vacuum chamber without electrical connection. The radius of the electrode is optimised to avoid the higher-order modes (HOMs) being trapped in the cavity.

To estimate the transverse and longitudinal impedances, the designed BPMs were modelled on the octagonal cross-section for HLS-Ⅱ. A high resolution hexagonal mesh is required for accurate discretization of many complex details with sizes <1 mm. Fig. 3 shows the longitudinal wake potentials of the BPM computed over a distance of 0.1 m at 10 lines per wavelength (in terms of CST parameters), but with two different constraints for the maximum longitudinal mesh step: the red and blue wake potentials correspond to a maximum longitudinal mesh step of 0.1 mm (250 million mesh cells per quarter of the 3D structure) and 0.01 mm (2500 million mesh cells per quarter of the 3D structure) respectively. As expected, a mesh with a smaller longitudinal step results in a better accuracy for the wake field solution: in particular, there is a significant reduction in the unphysical wake occurring ahead of the bunch.

We can find that the wake potentials computed directly by CST are compared with the wake potentials evaluated as a convolution of the charge distribution and the wake function (Fig. 4): the results are in good agreement, which indicates that the function has been computed with reasonable accuracy.

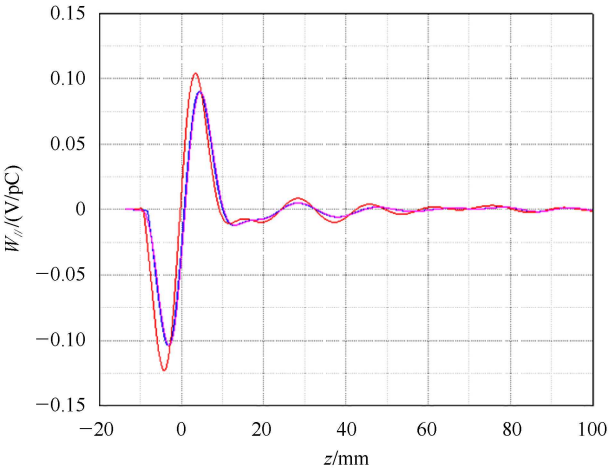

Fig. 3. (color online) Longitudinal wake potential of BPM computed by CST (red and blue lines); wake potential convoluted from the wake function (magenta line).

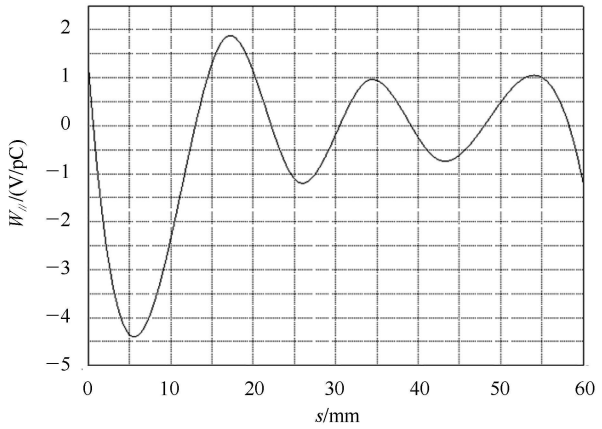

Fig. 4. (color online) Longitudinal wake function of the BPM.

3.4 Pump ports

In order to reduce the coupling impedance of the pump port, the pump port is designed with a mesh aperture to meet the required high pumping speed and continuity of vacuum chamber in the HLS-II storage ring.

There are four kinds of pump ports; their longitudinal impedance, loss factor and kick factor were calculated by the CST code.

3.5 Longitudinal feedback kicker

In order to damp the longitudinal coupled-bunch instabilities, we designed and installed a broadband longitudinal feedback kicker, which is a waveguide overloaded pillbox cavity with two input and two output ports. Meanwhile, there are two nose cones introduced to improve the shunt impedance of the cavity. This method leads to a strong coupling between the pillbox and the waveguides, which can help damp the harmful HOMs. In the calculation, we treated the interface of $x_{\min}$ $x_{\max}$ $y_{\min}$ and $y_{\max}$ as an outgoing wave guide port. Fig. 5 shows the longitudinal wake potential computed for the longitudinal feedback kicker. Compared to the wake potentials in the BPM and the longitudinal feedback kicker, we can find that later particles will suffer larger effects in the later component.

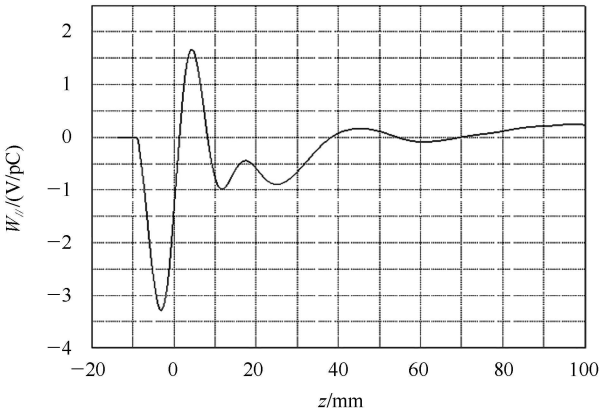

Fig. 5. (color online) Longitudinal wake potential of longitudinal feedback kicker.

3.6 Clearing electrodes

In the HLS-II storage ring, we designed the DC cleaning electrode to overcome ion trapping, which is one of the serious collective effects in low-energy storage rings. The clearing electrodes have a length of 525 or 615 mm, and are built in the vacuum chamber with four ceramic material supports and a high voltage electrode. Thus, the full height of the vacuum chamber is 43.5 mm, which is 3.5 mm higher than the common vacuum chamber.

3.7 RF cavity

At present, there is an old RF cavity installed in the HLS-II storage ring, which is an important source of impedance. A 3D model of the RF cavity was built using CST code. Its length was 0.472 m. Only the fundamental mode of the cavity has a high quality factor and shunt impedance, while all the other modes have low shunt impedance due to the HOMs dampers [11]. Fig. 6 shows the longitudinal wake potential computed for the RF cavity; we find that the wake potential also has a large value after a long distance.

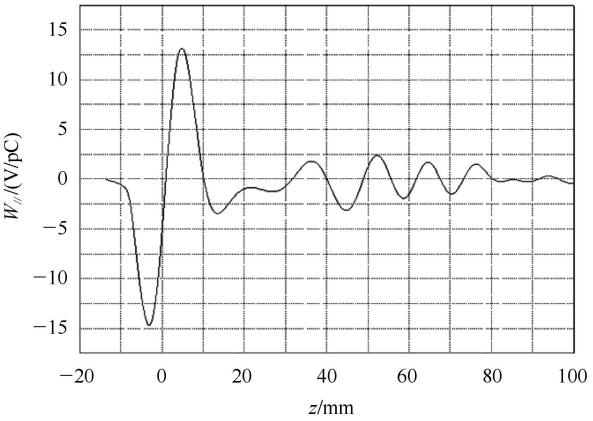

Fig. 6. (color online) Longitudinal wake potential of RF cavity.

3.8 Bending chamber

In a bending chamber, an electron beam moves along a curvilinear trajectory. Simulation of a curvilinear structure is impossible in CST. For this reason, a simplified rectilinear model of the HLS-II bending chamber including the octagonal beam channel, the pumping ports, and the BPM has been created (Fig. 7). Analysis of eigenwaves performed with CST shows that there is no longitudinal resonant mode excited in the structure.

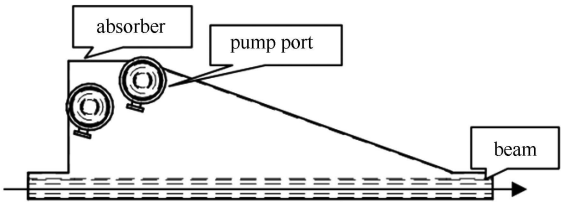

Fig. 7. (color online) Simplified rectilinear model of the HLS-II bending chamber.

3.9 Others

In addition to these main components, there are a large number of small discontinuities in the HLS-II storage ring, such as the connection between the flange and the vacuum chamber, shielded bellows, and slots for synchrotron radiation monitor and so on. In this paper, we used the CST code to set models and calculate the detailed wake fields and impedances. The results are shown in Fig. 8.

From Fig. 8, we find that the most significant wake potentials are produced by the pumping ports, the clearing electrodes, the longitudinal feedback kicker, the RF cavity and the bending chambers.

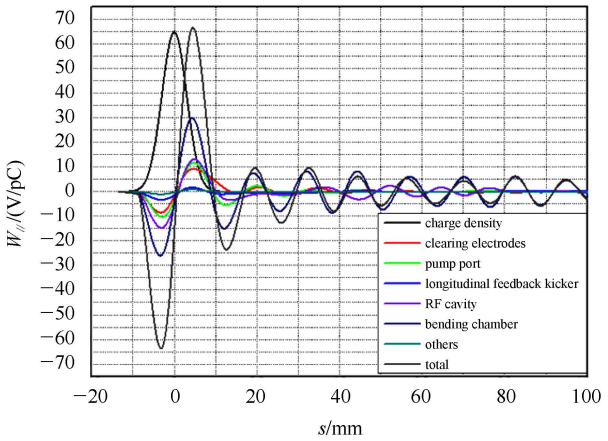

Fig. 8. (color online) Longitudinal wake potentials as a function of distance from the bunch head for various groups of elements.

4 Impedance budget

The impedance budget [12–14] of the HLS-II storage ring is shown in Table 2, where the longitudinal broadband impedance, the longitudinal loss factors, and the transverse kick factors are presented for each element. The major contributors to the impedance of the storage ring are the RF cavity, the pumping port chambers, the longitudinal feedback kicker and the flanges. The results indicate that the total longitudinal broadband impedance is about 0.82 Ω. Then we can obtain the broadband impedance model of the HLS-II storage ring as:

$$Z_{//}/n=0.819569j+\frac{4.5212(1+j)}{\sqrt{n}}+\frac{0.014774j}{n}+0.002497, \tag{7}$$

where the first term of the formula is the broadband impedance at low frequency, the second term is the resistive wall impedance, and the last two terms are the impedance of the coated ceramic vacuum chamber.

5 Instability threshold estimation

In this section, the total value of the longitudinal broadband impedance was used to study the single bunch instabilities in the HLS-II storage ring.

Table 2. Calculated impedance for components of the HLS-II storage ring.

component	N	$\lvert Z_{//}/n\rvert\Omega$	k/(V/pC)	k_x/(V/pC/mm)	k_y/(V/pC/mm)
RF cavity	1	0.018408	1.620064	2.361957	3.755356
pumping port	25	0.0046	1.3888	25.5577	30.9911
flange	59	0.2548	3.4787	1.8788	1.5853
BPM	36	0.0036	0.4301	1.6607	1.7164
clearing electrodes	32	0.0849	3.4887	72.4219	77.0221
bellows	16	4.6240e-05	0.1313	3.4647	3.4486
longitudinal feedback kicker	1	0.0095594	8.347e-001	8.221e-001	8.434e-001
bending chamber	8	0.4435	27.6218	18.6493	45.3778
others	—	1.5517e-04	0.6	2.8964	2 .7163
total	178	0.819569	39.59416	129.7136	167.4564

5.1 Microwave instability

When the peak current of a single bunch is higher than a threshold current, bunch lengthening and the energy spread increase are generated until the peak current is reduced to the current threshold. Meanwhile, microwave instabilities [15] also affect the brightness of the insertion device:

$$N_{\rm th}=\frac{(2\pi)^{3/2}\alpha_{\rm c}\sigma_{\varepsilon}^2(E/e)}{ce}\frac{\sigma_z}{|Z_{//}/n|}, \tag{8}$$

where the impedance $|Z_{//}/n|$ is calculated from the wake field using CST code, σ_z is the rms bunch length, σ_ε is the natural energy spread, and the value $N_{\rm th}$ given by Eq. (8) has been found to be 2.1637e+10. Then we can find that in the HLS-II storage ring, the threshold of single bunch current for microwave instabilities is 15.7 mA. Even considering the setting up error and some components missing in the estimation, we find that the threshold of single bunch current for microwave instability is larger than the design value.

5.2 Transverse mode coupling instability

When the beam current is increased, the coherent frequencies of head-tail modes are shifted and some of them may be coupled, which results in a fast beam instability. This is called the transverse mode coupling instability. For Gaussian bunches and broadband resonator impedance, $I_{\rm thresh}$ can be expressed with a kick factor $\kappa_\perp(\sigma_z)$ which eliminates the need for a bunch length cor-

rection factor: [15]

$$I_{\rm thresh}=\frac{C_1 f_{\rm s} E/e}{\sum\limits_i \beta_i \kappa_{\perp i}(\sigma_z)}. \quad (9)$$

The constant C_1 is about 8. Using the numerical value in Table 1, we can obtain a single bunch current threshold of 12.589 A, which is much larger than that for the longitudinal microwave instability. For a more exact calculation of the threshold we should use computer programs solving for the coherent modes, including the bunch lengthening and the potential-well deformation with the beam current. Nevertheless, we can conclude that the longitudinal microwave instability is much more significant in the storage ring.

6 Conclusions

The HLS-II storage ring broadband impedance and loss factor have been calculated. Contributions to the total broadband impedance from different groups of elements have been found. Meanwhile we estimate the instabilities based on the broadband impedance model, which do not seriously affect the beam quality. In future, we will use the broadband impedance to study the beam instabilities by tracking, and then we will calculate the narrowband impedance and study the coupled bunch instabilities for the HLS-II storage ring.

References

1 LI Wei-Min, XU Hong-Liang, WANG Lin, FENG Guang-Yao, ZHANG Shan-Cai, HAO Hao. The Upgraded Scheme of Hefei Light Source. AIP Conference Proceedings Vol. 1234 Issue 1, p764 June 2010
2 Computer Simulation Technology. http://www.cst.com/
3 CHAO A. Physics of Collective Beam Instabilities in High Energy Accelerators. New York: Wiley Inter Science. 1993
4 Ng K Y. Physics of Intensity Dependent Beam Instabilities, World Scientific Publishing Co. Pte. Ltd., 2006
5 Zotter B, Kheifets S. Impedances and Wakes in High Energy Particle Accelerators. London: W World Scientific, 1998
6 Bartolini R, Fielder R, Thomas C. Loss Factor and Impedance Analysis For the Diamond Storage Ring. Proceeding of IPAC'13. Shanghai, China
7 Stupakov G, HUANG Z. Space Charge Effect in an Accelerated Beam. SLAC-PUB-12768, August, 2007
8 Gluckstern R L, Zeijts J van, Zotter B. Coupling Impedance of Beam Pipes of General Cross Section. CERN SL/AP 92-25, June, 1992
9 Byrd J, Lambertson G. Resistive wall impedance of the B-factory. PEP-II AP Note 9-93, March 1993
10 Helmut Wiedemann Particle Accelerator Physics 3rd ed. New York: Springer Berlin Heidelberg, 2007
11 XU Hong-Liang, WANG Lin, LIU Jin-Ying, SUN Bao-Gen, HE Duo-Hui. Nuclear Techniques, 2003, **26**(5): 337–342
12 Danilov V. An Improved Impedance Model of Metallic Coatings. EPAC 2002. 1464–1466
13 ZHANG S Y. SNS Storage Ring Impedance. New York: Alternating Gradient Synchrotron Department Brookhaven National Laboratory, 1999: 15–16
14 Blednykh A, Krinsky S, Rose J. Coupling Impedance of CESR-B RF Cavity for the NSLS-II Storage Ring PAC. 2007
15 Alexander Wu Chao. Maury Tigner Handbook of Accelerator Physics and Engineering, World Scientific Publishing Co. Pte. Ltd., 2013